

# Mean Energy Density of Photogenerated Magnetic Fields Throughout the Epoch of Reionization

Jean-Baptiste Durrive<sup>1,2\*</sup>, Hiroyuki Tashiro<sup>2</sup>, Mathieu Langer<sup>1</sup> and Naoshi Sugiyama<sup>2,3,4</sup>

<sup>1</sup>*Institut d’Astrophysique Spatiale, CNRS, UMR 8617, Univ. Paris-Sud, Université Paris-Saclay, IAS, Bt. 121, 91405, Orsay, France*

<sup>2</sup>*Department of Physics and Astrophysics, Nagoya University, Nagoya 464-8602, Japan*

<sup>3</sup>*Kobayashi-Maskawa Institute for the Origin of Particles and the Universe, Nagoya University, Nagoya 464-8602, Japan*

<sup>4</sup>*Kavli Institute for the Physics and Mathematics of the Universe (Kavli IPMU), The University of Tokyo, Chiba 277-8582, Japan*

Accepted 2017 August 1; Received 2017 July 15; in original form 2017 May 23

## ABSTRACT

Magnetic fields are ubiquitous in the Universe. They seem to be present at virtually all scales and all epochs. Yet, whether the fields on cosmological scales are of astrophysical or cosmological origin remains an open major problem. Here we focus on an astrophysical mechanism based on the photoionization of the intergalactic medium during the Epoch of Reionization. Building upon previous studies that depicted the physical mechanism around isolated sources of ionization, we present here an analytic model to estimate the level at which this mechanism contributed to the magnetization of the whole Universe, thanks to the distribution of sources, before and alongside early luminous structure formation. This model suggests that the Universe may be globally magnetized to the order of, at least, a few  $10^{-20}$  G comoving (i.e. several  $10^{-18}$  G during the Epoch of Reionization) by this mechanism, prior to any amplification process.

**Key words:** magnetic fields—methods: analytical—dark ages, reionization, first stars—cosmology: theory.

## 1 INTRODUCTION

Observations indicate that magnetic fields are present in the Universe on a wide range of scales, from stars through galaxies to galaxy clusters (e.g. [Widrow 2002](#); [Beck 2011](#); [Vallée 2011](#); [Feretti et al. 2012](#); [Ryu et al. 2012](#); [Ferrario et al. 2015](#); [Beck 2016](#)). A relatively recent approach based on the observation of distant blazars repeatedly suggests that intergalactic filaments and cosmic voids too are magnetized to a level that could be at least as high as  $10^{-17} - 10^{-15}$  G (e.g. [Aleksić et al. 2010](#); [Neronov & Vovk 2010](#); [Dolag et al. 2011](#); [Tavecchio et al. 2011](#)). Note however that those conclusions depend strongly on assumptions, pertaining to the intrinsic properties of blazars, the extragalactic background light, systematic uncertainties, etc. (e.g. [Dermer et al. 2011](#); [Arlen et al. 2014](#)). In addition, note that plasma beam instabilities may be responsible (e.g. [Broderick et al. 2012](#); [Menzler & Schlickeiser 2015](#); [Chang et al. 2016](#)) for the non-detections of secondary electromagnetic cascades that are used to put lower limits on intergalactic magnetic fields (however, for an opposite viewpoint, see [Venters & Pavlidou 2013](#); [Sironi & Giannios 2014](#); [Kempf et al. 2016](#), for instance). On the other side of the strength range, upper limits on intergalactic

magnetic fields of the order of  $10^{-9}$  G are obtained from the Cosmic Microwave Background, both temperature and polarization anisotropies and spectral distortions (e.g. [Chluba et al. 2015](#); [Planck Collaboration 2016c](#); [Zucca et al. 2017](#)), as well as from various large-scale structure observations (e.g. [Blasi et al. 1999](#); [Pandey & Sethi 2013](#); [Pshirkov et al. 2016](#); [Brown et al. 2017](#)).

According to the current paradigm, those fields were first generated as weak seeds that were later on amplified, perhaps first on small scales within early galaxies through a small-scale dynamo (e.g. [Schober et al. 2013](#)) or in the post-recombination intergalactic medium through collisionless plasma instabilities (e.g. [Falceta-Gonçalves & Kowal 2015](#)). Had they been generated with strengths larger than a few nano-Gauss, magnetic fields would have noticeably affected subsequent structure formation ([Wasserman 1978](#); [Kim et al. 1996](#); [Tashiro & Sugiyama 2006](#); [Varalakshmi & Nigam 2017](#)). Such seed fields were then reorganized through adiabatic compression and various dynamo mechanisms during or after structure formation (e.g. [Brandenburg & Subramanian 2005](#); [Arshakian et al. 2009](#); [Ryu et al. 2012](#)). The origin of the seed magnetic fields however, particularly on the largest scales, is still uncertain, despite the many magnetogenesis mechanisms that have been proposed in the literature (see for instance [Widrow 2002](#); [Kulsrud & Zweibel](#)

\* E-mail: jean.baptiste.durrive@e.mbox.nagoya-u.ac.jp

2008; Ryu et al. 2012; Widrow et al. 2012; Durrer & Neronov 2013, for reviews). Many of those mechanisms are based on high energy physics, beyond the standard model, possibly operating in the early Universe (see Widrow et al. 2012; Durrer & Neronov 2013; Subramanian 2016, for recent reviews). In the post-recombination Universe, classical plasma physics is also efficacious to generate magnetic field seeds through plasma instabilities (e.g. Gruzinov 2001; Schlickeiser & Shukla 2003; Medvedev et al. 2006; Lazar et al. 2009; Bret 2009; Schlickeiser 2012), the Biermann (1950) battery (e.g. Pudritz & Silk 1989; Subramanian et al. 1994; Ryu et al. 1998; Gnedin et al. 2000; Naoz & Narayan 2013) or the momentum transfer of photons or protons to electrons (e.g. Harrison 1970; Mishustin & Ruzmaikin 1972; Harrison 1973; Birk et al. 2002; Langer et al. 2003, 2005; Fenu et al. 2011; Saga et al. 2015). Another plausible possibility is that magnetic fields were generated within collapsed structures, and then ejected on larger scales into the intergalactic medium by galactic winds, outflows and AGN jets (e.g. Rees 1987; Daly & Loeb 1990; Kronberg et al. 1999; Furlanetto & Loeb 2001; Beck et al. 2013).

In Durrive & Langer (2015) (DL15 hereafter; see also Langer et al. 2005), the authors explored in some depth the generation of magnetic fields on large scales induced by the photoionization of the intergalactic medium (IGM) during the Epoch of Reionization (EoR). They have shown that, thanks to ionization-induced charge separation in an inhomogeneous medium, an electric field possessing a curl component is generated over large distances, thus creating magnetic fields. Typically,  $10^{-23}$ – $10^{-18}$  G magnetic fields arise on scales which, depending on the nature of the ionizing sources, range from kiloparsecs (Population III stars) and tens of kiloparsecs (primordial galaxies) to megaparsecs (quasars). They have also shown that the scales over which the strengths of the generated magnetic fields are significant are of the order of the average distance between ionizing sources. Thus, this mechanism is naturally able to magnetize the entire Universe at redshifts  $z \simeq 30$  to  $z \simeq 6$ .

In this paper, in order to evaluate the cosmological importance of this mechanism, we estimate the level of global magnetization of the Universe it produces. This naturally depends on the distribution of ionizing sources (namely the typical separation between their Strömgren spheres), their spectral properties, the epochs at which they appear and the distribution of density inhomogeneities in the IGM. We estimate the mean magnetic strength injected into the IGM by all the sources emitting light above the hydrogen ionization threshold throughout the EoR, with a simple model.

The authors in DL15 modelled the clumpiness of the IGM as a distribution of baryon overdense clouds. They derived a very detailed formula giving the strength of the magnetic field generated within and around a given overdense cloud surrounding an ionizing source. However the latter expression is rather involved. Fortunately, they also identified the characteristic length scales of the problem useful for modelling simply the magnetized area around that given overdensity. Building upon this, in this paper, we use the Press-Schechter formalism (Press & Schechter 1974) to estimate the statistical distribution of ionizing sources and of overdensities around these sources. More precisely, we consider dark matter (DM) haloes which are massive enough to host luminous sources and DM overdensity regions which

have not yet collapsed but contain diffuse baryonic overdense clouds. Then, using an approximate expression for the magnetic field generated around overdensities in DL15, we may estimate the magnetic field generated by all the sources forming during the EoR. Here, for simplicity, we focus on primordial galaxies only as ionizing photon sources. In fact, it has been suggested that these galaxies are the dominant contributors to reionization (e.g. McQuinn 2016, and references therein), a hypothesis recently strengthened by the interpretation of Cosmic Microwave Background data (Planck Collaboration 2016d). Therefore, this approach should give us a realistic estimation of the magnetization level obtained at the end of the EoR.

This paper is organized as follows. First, in section 2, we model the magnetic field generated around one source, due to the presence of one cloud and then due to the presence of a distribution of clouds. Then, in section 3, we estimate the global field generated by a distribution of such sources surrounded by clouds during EoR. Conclusions are discussed in section 4. Through this paper, we use the Planck reference cosmology (Planck Collaboration 2016b), namely  $\Omega_b h^2 = 0.02226$ ,  $\Omega_c h^2 = 0.1197$  and  $h = 0.6781$ .

## 2 MAGNETIC FIELD GENERATION AROUND ONE SOURCE

In DL15 the authors computed in full details (strength, field line geometries, spatial extent) the magnetic field generated around a single isolated source as it occasionally ionizes the neutral IGM outside its Strömgren sphere. They showed that three crucial ingredients source magnetic fields: local inhomogeneities in the electron fraction, anisotropies of the Strömgren sphere and inhomogeneities in the neutral Hydrogen density. As in this paper, we will focus on the contribution from inhomogeneities here, leaving the rest for future work. Note that this already gives us a hint that the estimation deduced here may be an underestimation of the global field strength (cf. section 4 for more details). Also, in DL15, the authors performed numerical applications relevant in the cosmological context of EoR, by considering several types of sources (first stars, primordial galaxies and quasars), operating at various epochs. One of the outcomes of their exploration is that one has to be careful with the naive intuition that, the more powerful the source is, the stronger the generated magnetic fields are. Indeed, a powerful source emits many photons with short mean free paths (i.e. of frequency close to  $\nu_0$ ) generating a large Strömgren sphere. Photons with large mean free paths hence first have to propagate a large distance before reaching the neutral IGM (where they participate to the present mechanism). Therefore they are highly diluted (by geometry), which is why for a given spectrum a very powerful source will induce magnetic fields which are in fact weak. Numerically, they concluded that primordial galaxies constitute the best compromise between power and dilution. This is interesting since it is precisely primordial galaxies that are nowadays believed to have been the main drivers of cosmic reionization. For these reasons, in the present analysis we will consider only primordial galaxies as ionizing sources. Following DL15, we assume that sources are characterized by a power-law luminosity in a certain fre-

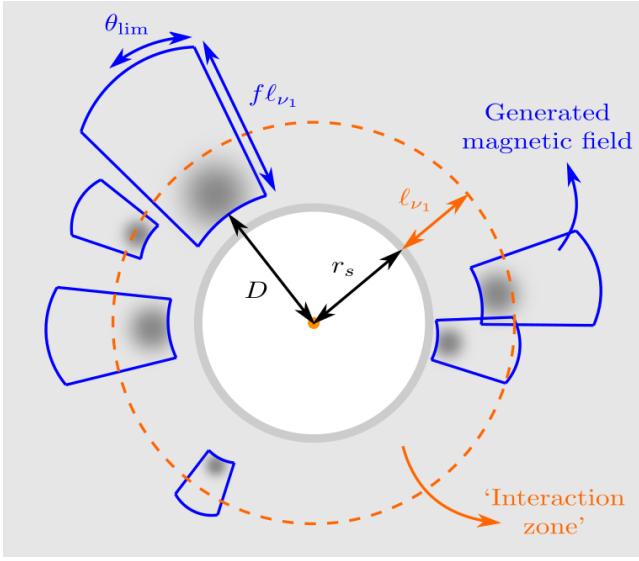


**Figure 1.** Illustration of the magnetic field generated by a luminous source (the orange spot) as it photoionizes the neutral IGM (the light grey region) during EoR. The white region corresponds to the Strömgren sphere ( $r \leq r_s$ ) of the source and the dark grey spots are overdense clouds modelling the clumpiness of the IGM. The orange dashed line delimits the ‘interaction zone’ ( $r_s \leq r \leq r_s + \ell_{\nu_1}$ ), i.e. the volume containing the clouds that are close enough to the source to participate significantly to the magnetogenesis, because further away the number of photoionizations is too small. In our calculation we thus take into account only clouds inside this zone. Magnetic fields are generated inside and behind these clouds, as represented by the blue frames [corresponding formally to equation (4)], and have strengths well approximated by equation (3) (plotted in Fig. 2). This modelling abbreviates efficiently the general and detailed results of DL15.

quency range:

$$L_\nu = L_0 \left( \frac{\nu}{\nu_0} \right)^\alpha \quad \text{for } \nu \in [\nu_0, \nu_1], \quad (1)$$

where  $\nu_1$  is the cut-off frequency and we set  $\nu_1 = 4\nu_0$  with  $\nu_0$  being the Hydrogen ionization threshold. Parameters  $L_0$  and  $\alpha$  depend on the model of ionizing photon sources. In this paper, the sources considered are primordial galaxies consisting of Population II stars, with typically  $L_0 = 3 \times 10^{25}$  erg/s/Hz and  $\alpha = -2$ . See Sec. 3.1 for more details.

## 2.1 One cloud

In DL15, acknowledging that the results they obtained in full generality were quite involved, the authors have extracted from them the relevant length scales by considering simple baryon cloud inhomogeneities with a Gaussian profile as toy models. Pursuing in this direction, we will here simplify a little step further their expressions to obtain an efficient but still accurate expression for the fields generated around a cloud near a given source. As illustrated in Fig. 1, we will retain only the following assumptions: (i) magnetic fields are generated essentially only by the baryon overdense clouds that are close enough to the source, i.e. that are within what we shall call the ‘interaction zone’, defined as the shell of thickness  $\ell_{\nu_1}$  around the Strömgren sphere, where  $\ell_{\nu_1}$  is the

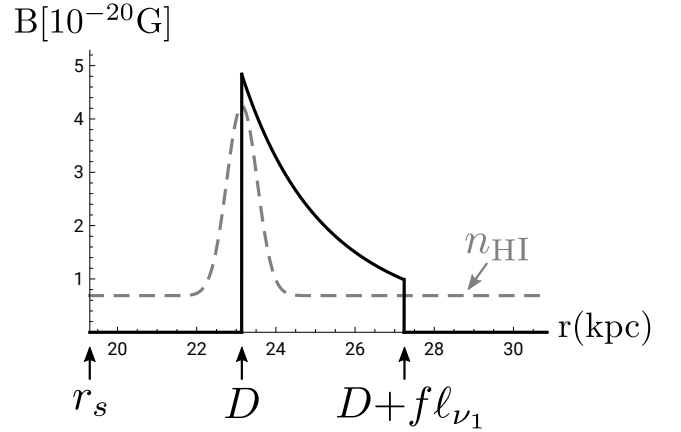


**Figure 2.** Example of the profile given by equation 3. The grey dashed line is added to illustrate the position and shape of the overdensity (‘cloud’) inducing this magnetic field.

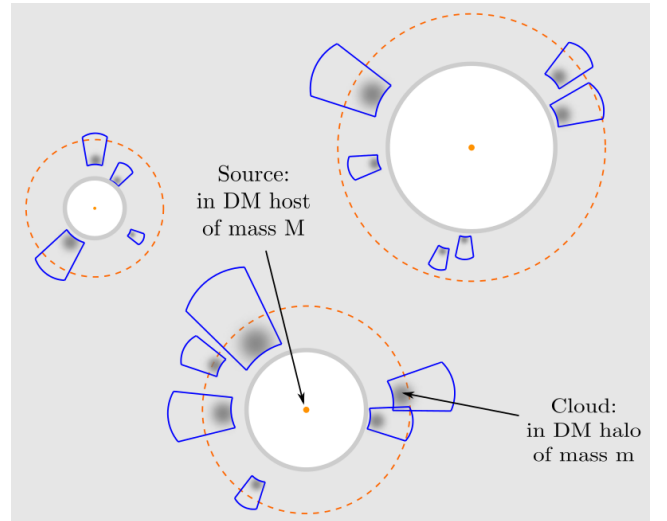


**Figure 3.** This mechanism operates around each source all along the EoR. In this paper we compute the mean magnetic energy density generated (illustrated by the blue frames) in the whole Universe throughout this epoch. We do so by considering that the distribution of sources and the distribution of the (baryonic) clouds surrounding them are given by the distribution of DM haloes in which they are embedded. Conventions in this figure are the same as in Fig. 1.

mean free path of the most energetic photons emitted by the source [of frequency  $\nu_1$ , cf. equation (1)], and (ii) the magnetic field is generated about a cloud at distance  $D$  with a simple Gaussian density profile of neutral hydrogen

$$n_{\text{HI}} = \bar{n} \left( 1 + \delta_0 e^{-\frac{(\tilde{r}-\tilde{D})^2}{2\sigma^2}} \right), \quad (2)$$

where  $\delta_0$  is the central amplitude of the density contrast (an overdensity for  $\delta_0 > 0$ , an underdensity for  $-1 \leq \delta_0 < 0$ ) and  $\sigma$  is the width of the cloud, (iii) the generated magnetic field strength is well approximated by the following

profile (obtained from equations (39) and (41) of DL15)

$$B_{\sigma, \delta_0, D}(r, \theta, \varphi) = B_{\max} \left( \frac{r - r_s + \sqrt{2\pi/e} \delta_0 \sigma}{D - r_s + \sqrt{2\pi/e} \delta_0 \sigma} \right)^{\frac{\alpha-5}{3}} \times \left( \frac{r}{D} \right)^{-3} \mathcal{G}(r, \theta; D, \theta_{\text{lim}}), \quad (3)$$

where  $B_{\max}$  is defined below. This profile is plotted in Fig. 2. In the above equation,  $\mathcal{G}$  is a function delimiting the specific region in which  $B$  can be considered as non-negligible. As detailed and illustrated on the right-hand panel of figure 2 of DL15, it is relevant to take the following simple expression for the function  $\mathcal{G}$

$$\mathcal{G}(r, \theta; D, \theta_{\text{lim}}) = \Theta(r-D)\Theta(r-r_s)\Theta(\theta_{\text{lim}}-\theta)\Theta(D+f\ell_{\nu_1}-r), \quad (4)$$

i.e. using Heaviside step functions to delimit this region. This is illustrated by the blue frames surrounding each cloud in Fig. 1.

In DL15, it was shown that the strength of the generated magnetic fields reaches its maximum at  $r = D$ . It is given by [cf. equation (39) in DL15]

$$B_{\max} = t_* \frac{1}{15} \sqrt{\frac{2}{\pi e}} \frac{\sigma_0^2 L_0 \nu_0}{q x_e D^2} n_{\text{HI}} \delta_0 F(D, \sigma), \quad (5)$$

where  $t_*$  is the lifetime of the hard photon emitting phase of the source, set to  $t_* = 100$  Myr in our model, and  $F(D, \sigma)$  is the coefficient representing the geometrical effects of the cloud

$$F(D, \sigma) = \Gamma\left(\frac{5-\alpha}{3}\right) \left( \frac{D-r_s + \sqrt{\pi/2e} \delta_0 \sigma}{\ell_{\nu_0}} \right)^{(\alpha-5)/3} - \Gamma\left(\frac{6-\alpha}{3}\right) \left( \frac{D-r_s + \sqrt{\pi/2e} \delta_0 \sigma}{\ell_{\nu_0}} \right)^{(\alpha-6)/3} \quad (6)$$

where  $\Gamma$  is the gamma function. For  $r < D$  the field is smaller than  $B_{\max}$ , but non-vanishing. However, for simplicity, we take it here equal to zero. For  $r > D$  the strength decays as the product of power laws in  $r$  given by equation (3), but we introduce a cut-off distance  $f\ell_{\nu_1}$ , cf. equation (4), after which we consider the field to be negligible because it is not physical to consider infinitely large distances. Also, the role of the factor  $f$  is to let us control this cut-off, measuring it in units of the relevant scale  $\ell_{\nu_1}$ . Numerically, we observe that the results we obtain below are insensitive to values of  $f$  greater than typically 2.

In equation (3), we are considering that the field is azimuthally symmetric since there is no dependence on the angle  $\varphi$ , and that the dependence in the angle  $\theta$  is piecewise, where the angle  $\theta_{\text{lim}}$  is given by

$$\theta_{\text{lim}} = \arcsin\left(\frac{3\sqrt{3}}{2} \frac{\sigma}{D}\right). \quad (7)$$

Although in reality the magnetic fields have smooth, angular variations detailed in DL15, these are fair assumptions since, through the truncation given in equation (4), we already consider only a restricted volume where the magnetic field is generated.

We may now express the energy injected into the IGM in the form of magnetic fields due to one cloud. It is the integral of the magnetic energy density  $B^2/8\pi$  (Gaussian units) over the whole volume in which the field is generated,

that is

$$E_{\sigma, \delta_0}(D) = \int_0^{\theta_{\text{lim}}} d\theta \sin\theta \int_0^{2\pi} d\varphi \int_D^{D+f\ell_{\nu_1}} dr r^2 \frac{B_{\sigma, \delta_0, D}^2}{8\pi}. \quad (8)$$

## 2.2 Distribution of clouds

So far we have estimated the magnetic field generated behind a baryon cloud around a luminous source. However, in reality, an entire distribution of clouds is present around a source, as illustrated in Fig. 3, and the resultant generated magnetic fields are the sum of the fields generated by each cloud. To evaluate the total magnetic fields generated through this mechanism, it is essential to estimate the distribution of clouds quantitatively. Therefore, here we make the following assumptions: (1) the luminous source is hosted in a DM halo whose mass is noted  $M$  and (2) each baryon cloud is contained in a DM overdense region with mass  $m$  which has not yet collapsed. Hereafter, we call the DM haloes of mass  $M$  ‘hosts’ and the uncollapsed DM overdense regions ‘DM clouds’. Note also that, since a DM cloud is only weakly overdense, we consider that the DM density profile in a DM cloud is the same as that of the baryons it contains, i.e. a Gaussian density profile.

Under this assumption, we can calculate the distribution of the baryon clouds around a source by considering the distribution of DM overdense regions around a DM halo. Based on the definition of the correlation function (Peebles 1980), the probability of finding a DM cloud of mass  $m$  within a spherical shell of volume  $4\pi D^2 dD$ , at a distance  $D$  from a DM host halo of mass  $M$ , is given by

$$d^2 P(D, m|M) = \frac{dn_m}{dm} (1 + b_h(M)b_c(m)\zeta(D)) 4\pi D^2 dD dm, \quad (9)$$

where  $dn_m/dm$  is the mass function of the DM clouds, with mass  $m$ . To calculate  $dn_m/dm$ , we use the Press-Schechter (PS) formalism (Press & Schechter 1974). The function  $\zeta$  is the linear matter density correlation function, and two bias parameters,  $b_h(M)$  and  $b_c(m)$ , are introduced, respectively, for the host halo of mass  $M$  and the DM cloud of mass  $m$ , to represent the enhancement of these overdensity peaks with respect to the background mass overdensity (cf. Mo et al. 2010, for instance). To obtain the total magnetic energy generated around the source, we simply need to add the contribution of each cloud. But, as shown in equation (8), the generated magnetic fields are characterized by the parameters  $(\sigma, \delta_0)$  of the profile of the cloud (representing respectively its characteristic size and the value of its central overdensity), and not directly the mass  $m$ . However, since we assume that clouds have Gaussian density profiles, we can easily calculate its mass and use parameters  $(m, \delta_0)$ , instead of  $(\sigma, \delta_0)$ . The PS formalism provides the mass function of clouds with  $(m, \delta_0)$ , given the linear density contrast corresponding to  $\delta_0$ . Now, as mentioned above, while a host is a collapsed object, a cloud is not collapsed. Here we set the critical linear density contrast for a cloud as  $\delta_{ch} = 1.05$  corresponding to the turn-around time, and assume that all clouds have the central density  $\delta_0 = 5.55$  corresponding to the non-linear density contrast at the turn-around time. In the remainder of the paper we will then note  $E_m$  the magnetic energy corresponding to  $E_{\sigma, \delta_0}$  of equation (8). We may

then sum up the contribution of all the clouds surrounding the source, and conclude that to each source in a halo of mass  $M$  corresponds a magnetic energy

$$E_M = \int_{r_s}^{r_s + \ell_{\nu_1}} \int_{m_{\min}}^{m_{\max}} E_m(D) d^2P(D, m|M). \quad (10)$$

The boundaries of the first integral in this equation express the fact that only the clouds inside the ‘interaction zone’ (cf. Fig. 1) generate significant magnetic fields and are taken into account. Let us now discuss the boundaries of the second integral, namely  $m_{\min}$  and  $m_{\max}$  for the mass of the clouds.

For the upper bound, we have two constraints. First, a cloud that is very large may turn out to be totally opaque, even to the most energetic photons emitted by the source. It then does not contribute efficiently to the magnetization of the IGM since no photon passes through them. More precisely, when light crosses a cloud modelled as a Gaussian overdensity  $\delta_0$  of width  $\sigma$  embedded in a background density  $\bar{n}$ , the radiation intensity behind the cloud is attenuated by a factor  $\epsilon = \exp(-\sigma_{\nu_1} \int n_{\text{HI}} dr)$  with respect to the ambient radiation field. For instance  $\epsilon \simeq \exp\left[-(1 + \delta_0) \frac{2\sigma}{\ell_{\nu_0}}\right]$  for  $\nu = \nu_0$ , and since we fix  $\delta_0$ , we get a relation between  $\sigma$ , and therefore on the mass of the cloud, for a given attenuation factor  $\epsilon$ . In this paper, we set  $\epsilon < 1$  as an upper bound for the cloud mass. A second constrain simply comes from the fact that, located at a distance  $D$  from the source of ionizing photons, the width of a cloud cannot be larger than  $D - r_s$ , otherwise it would encroach on the Strömgren sphere of the source. Thus, we take for  $m_{\max}$  in equation (10) the minimum of these two upper bounds. On the other hand, very small DM overdensities are unable to host diffuse baryons, due to pressure effects of the latter. Since the sound speed, and thus the Jeans mass may change significantly during the time it takes for an overdensity to grow, Gnedin & Hui (1998) showed that the correct mass scale to consider is the so-called ‘filter mass’  $M_F$  which is of the order of  $2 - 3 \times 10^4 M_\odot$  and varies only a little with redshift until reionization is complete (Naoz & Barkana 2007). However, the streaming velocity between gas and DM, left over from recombination, may have the effect of increasing  $M_F$  by roughly an order of magnitude (Tselikhovich et al. 2011). In the following, we take  $m_{\min} = 10^4 M_\odot$  for simplicity, and we keep in mind that it may be roughly 10 times larger. We will discuss the sensitivity of our results to these mass bounds in section 3.2.

### 3 MAGNETIC ENERGY DENSITY GENERATED IN THE IGM

In the previous section we have computed explicitly the magnetic energy density generated around an isolated source surrounded by neutral clouds. Now, in order to evaluate the field generated throughout the IGM, we need to take into account the cosmological context in which sources evolve. This consists in three steps. First, since sources are contained in DM haloes of mass  $M$ , we use the PS formalism to estimate their number density. Second, we need to take into account the fact that not all DM haloes contain luminous sources. We introduce in our model the rate at which DM haloes can ‘switch on’ sources, so as to make it consistent with an

important observational constraint on EoR, namely the optical depth parameter deduced from the Planck 2015 data (Planck Collaboration 2016a,b). Indeed, if too many hosts contain sources, then the EoR ends too soon compared to what observations suggest, and vice versa. Third, we must account for the fact that sources switching-on early are isolated, embedded in an essentially neutral medium, and thus generate the energy computed in the previous section, while those appearing towards the end of EoR hardly contribute to the magnetization of the IGM because not much of the neutral gas is left due to the overlapping of cosmological Strömgren. We do so by introducing the ionization fraction of the IGM as follows.

#### 3.1 Ionization of the IGM

Let us now compute the ionized volume associated with DM haloes. Assuming a universal baryon-to-dark mass fraction, a DM halo of mass  $M$  contains a mass  $M\Omega_b/\Omega_m$  of baryons. However, not all this mass is converted into the stars constituting the ionizing source. We introduce a parameter  $f_*$  representing the fraction of baryons converted into stars. With  $\dot{N}_*$ , the rate of ionizing photons emitted per baryons, the ionizing photon production rate from a DM halo with mass  $M$  is given by

$$\dot{N}_{\text{ion}} = f_* f_{\text{esc}} \dot{N}_* \frac{\Omega_b}{\Omega_m} \frac{M}{m_p}, \quad (11)$$

where  $f_{\text{esc}}$  is the escape fraction introduced to account for the fact that only a fraction of the emitted photons participate to the ionization of the IGM. The rate  $\dot{N}_*$  depends on the models of ionizing photon sources, but a typical value is  $\dot{N}_* = 40 \text{ Myr}^{-1}$  (e.g. Loeb & Furlanetto (2013), which is consistent with the Yggdrasil model<sup>1</sup> used in DL15 (Zackrisson et al. 2011), which uses the Schaerer (2002) and Raiter et al. (2010) single stellar populations). Once  $\dot{N}_{\text{ion}}$  is obtained for a DM halo of mass  $M$ , we get the corresponding luminosity  $L_0$  in equation (1) from

$$\dot{N}_{\text{ion}} = \int_{\nu_0}^{\infty} \frac{L_\nu}{h\nu} d\nu, \quad (12)$$

where we set the spectral index  $\alpha = -2$ .

We evaluate the size of the ionized bubble produced by the source by computing the corresponding Strömgren radius (e.g. Loeb & Furlanetto 2013, and considerations in DL15):

$$r_s = \left( \frac{3\dot{N}_{\text{ion}}}{4\pi\alpha_B C n_{\text{HI}}^2} \right)^{1/3}, \quad (13)$$

where  $\alpha_B$  is the case-B recombination coefficient ( $\alpha_B = 2.6 \times 10^{-13} \text{ cm}^3 \text{ s}^{-1}$  at a gas temperature of  $10^4 \text{ K}$ ),  $n_{\text{HI}}$  is the neutral hydrogen number density in the IGM, and  $C$  is the hydrogen clumping factor. The clumping factor depends on the redshift and is yet rather poorly constrained. We use the fitting function  $C(z) = 27.466 \exp(-0.114z + 0.001328z^2)$  obtained by Mellema et al. (2006). Putting everything together, we can obtain the volume of the ionized bubble produced by a DM halo of mass  $M$  containing ionizing sources,

<sup>1</sup> <http://ttt.astro.su.se/~ez/>

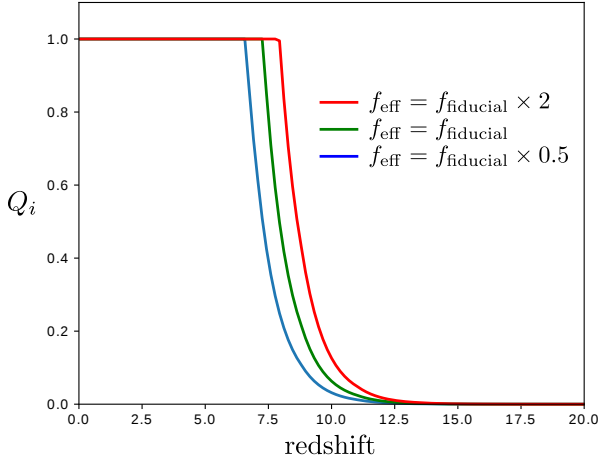


**Figure 4.** Redshift evolution of the ionization fraction  $Q_i$  in our reionization model. The red, green and blue curves are respectively for  $f_{\text{eff}} = 2 \times f_{\text{fiducial}}$ ,  $f_{\text{fiducial}}$ ,  $0.5 \times f_{\text{fiducial}}$ , where  $f_{\text{fiducial}} = 1.5 \times 10^{-3}$  is the value of  $f_{\text{eff}}$  in our fiducial model (green curve). The blue curve corresponds to a Universe in which sources are weakly ionizing (low escape fraction and/or low star formation, i.e. low  $f_{\text{eff}}$ ) while the red curve corresponds to a model with strongly ionizing sources. The blue and red cases are the extreme cases admissible to stay reasonably close to both the measurements of the end of Reionization, and to the measurements of the optical depth (cf. Fig. 5).

namely

$$V_{\text{ion}}(M) = \frac{f_* f_{\text{esc}} \dot{N}_* \Omega_b}{\alpha_B C n_{\text{HI}}^2} \frac{M}{\Omega_m m_p}. \quad (14)$$

We are now ready to compute the ionized fraction of the Universe at a given time  $t$ . Ignoring the recombination process inside ionized bubbles, it is given by the volume filling factor of ionized bubbles,

$$Q_i(t) = \int_{t_0}^t dt \int_{M_*}^{M_{\text{max}}} dM V_{\text{ion}}(M) g_{\text{gl}} \frac{dn_M}{dM}, \quad (15)$$

where the parameter  $g_{\text{gl}}$  is the rate at which sources switch on in DM haloes and  $dn_M/dM$  is the mass function of DM haloes with mass  $M$ . The lower halo mass limit is set by the requirement that the DM hosts contain galaxies. Thus, the minimum mass in the above equation is the mass of haloes whose virial temperature is below the atomic cooling threshold,

$$M_* = 5 \times 10^7 h^{-1} \left( \frac{\mu}{0.6} \right)^{-3/2} \Omega_m^{-1/2} \left( \frac{1+z}{10} \right)^{-3/2} M_{\odot}, \quad (16)$$

where  $\mu$  is the mean atomic weight of the gas and  $\Omega_m$  the present-day matter density (e.g. Glover 2013). The time  $t_0$  is the time at which the first sources switch on, corresponding to a redshift that we take equal to  $z = 20$  in the following since we are considering primordial galaxies.

To perform numerical applications, we must choose the values of  $f_*$ ,  $f_{\text{esc}}$  and  $g_{\text{gl}}$ . However, the values of the parameters  $f_*$  and  $f_{\text{esc}}$  are uncertain and depend on both the redshift and the source of ionizing photons. For example, observations of galaxies at  $z \sim 3$  by (Iwata et al. 2009) indicate an escape fraction of  $f_{\text{esc}} < 0.1$  while numerical sim-

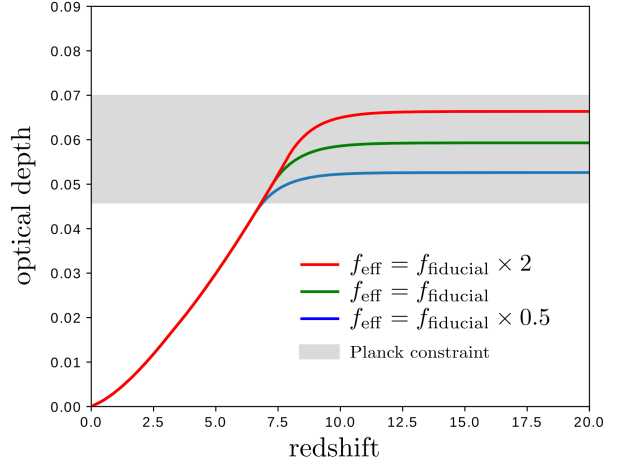


**Figure 5.** Evolution of the integrated Thomson optical depth  $\tau$  to the CMB in our model, in complement to Fig. 4. We choose values of  $f_{\text{eff}}$  to stay within the error bars of the most recent result  $\tau = 0.058 \pm 0.012$  released by the Planck Collaboration (2016d).

ulations (Wise & Cen 2009; Hayes et al. 2011; Wise et al. 2014) suggest that it can be larger than 0.1 at high redshifts. A natural requirement for these parameters is that our model of Reionization must be consistent with the observations and the simulations related to the EoR. Here, combining these two parameters, we define  $f_{\text{eff}} \equiv f_* f_{\text{esc}}$  and set  $f_{\text{eff}} = 1.5 \times 10^{-3}$  in our fiducial model. For the parameter  $g_{\text{gl}}$ , we take it equal to zero at redshifts greater than 20, and  $g_{\text{gl}} = 2 \times 10^{-8} \text{ yr}^{-1}$  at  $z \leq 20$ , in order for our fiducial model to be consistent with the measurements of the ionized fraction during EoR.

Fig. 4 shows the redshift evolution of the ionized fraction  $Q_i$  for different  $f_{\text{eff}}$ . In the figure, the green line represents our fiducial model in which the EoR ends at  $z = 7$ . Note that the value assigned to  $g_{\text{gl}}$  is in fact quite natural: the corresponding time-scale is  $g_{\text{gl}}^{-1} = 50 \text{ Myr}$ , and since the period between  $z = 20$  and 7 is roughly half a Giga-year long, with this choice we are considering a Reionization driven by about 10 generations of galaxies. Of course, taking a redshift independent  $g_{\text{gl}}$  is a simplification since for instance the metal enrichment process caused by supernovae explosions modifies the galaxy formation rate. However, since we consider galaxies and not Population III clusters, we expect that this metal enrichment process has already been saturated, and therefore it is a fair assumption to take  $g_{\text{gl}}$  constant with redshift. For consistency checks, we also computed the Thomson optical depth to the CMB and, as shown in Fig. 5, our fiducial Reionization model is perfectly consistent with the Planck cosmological result,  $\tau = 0.058 \pm 0.012$  (Planck Collaboration 2016d).

In order to explore the role played by the parameter  $f_{\text{eff}}$ , we also consider two other cases. Red lines in Figs 4 and 5 correspond to a Universe in which galaxies are strongly ionizing, i.e. they emit ionizing photons at high rates (high  $\dot{N}_{\text{ion}}$ , high  $f_{\text{eff}}$ ), either because stars are formed very efficiently (high  $f_*$ ) or because photons are not trapped (high  $f_{\text{esc}}$ ). It is thus natural to see in Fig. 4 that they reionize the Universe faster than in the fiducial model, and that in

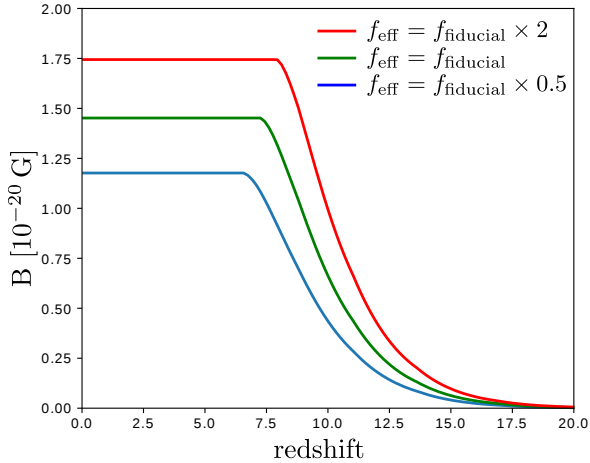


**Figure 6.** Evolution with redshift of the mean comoving magnetic field accumulated in the IGM generated by the first galaxies for different reionization parameters, computed from formula (17). As detailed in Figs 4 and 5, the green curve corresponds to our fiducial model, the blue curve corresponds to a Universe in which sources are weakly ionizing, and the red curve to strongly ionizing sources. Note that these curves correspond to comoving values, so that the physical magnetic strength is of several  $10^{-18}$  G during EoR, without taking any amplification process into account.

this case the optical depth is larger since more electrons are freed sooner. On the other hand, blue lines correspond to the opposite situation. Fig. 5 shows that, in both cases, the optical depth remains within the error bars of the Planck recent results.

### 3.2 Results

We can now calculate the mean magnetic energy density (physical) generated by photoionizations during the EoR. For simplicity, we assume that magnetic flux is frozen in the IGM and we do not consider any possible dissipation or amplification. Thus, magnetic fields are continuously generated in the IGM during the EoR and are subsequently diluted adiabatically by cosmic expansion once they reach their maximum strength.

Accordingly, with equations (A2), (A3) and (A4), we eventually obtain that the mean physical magnetic energy density generated by photoionizations during EoR evolves with redshift as

$$\frac{B_p^2(z)}{8\pi} = (1+z)^4 \int_z^{z_0} dz' \frac{1-Q_i}{(1+z')^5 H} \int_{M_*}^{M_{\max}} dM E_M g_{\text{gl}} \frac{dn_M}{dM}, \quad (17)$$

where  $z_0$  (taken equal to 20 here) is the redshift at which the entire process sets in (full derivation provided in section A). Since by assumption there are no magnetic fields initially, we have set  $B_p(z_0) = 0$ .

Let us explain where the  $1 - Q_i$  factor comes from. The magnetic energy calculated in equation (10), giving the energy in magnetic fields generated around a single source, must be integrated over the distribution of DM haloes. However, ionized bubbles of individual sources start to overlap

around the end of the EoR. Since our magnetic field generation mechanism takes place only in the neutral IGM, the efficiency of magnetic field generation actually decreases as the reionization process proceeds. Accordingly, the factor  $1 - Q_i(z)$  reduces the generated magnetic field energy as time increases, and terminates the whole process when Reionization is completed.

In Fig. 6, we plot the comoving strength of the generated magnetic field,  $B_c = B_p/(1+z)^2$ , as a function of redshift, with various Reionization histories (the various curves corresponding to those in Figs 4 and 5). The global trend of each curve can be naturally explained as follows. Above  $z = 20$  there are no galaxies, so that the strength is equal to zero, and then as time passes, galaxies form and their radiation generates magnetic fields, i.e. a tiny fraction of their radiation energy is converted into magnetic energy, which accumulates in the IGM, so that the curves rise with decreasing redshift. Once the Universe is totally ionized, the generation stops and a plateau is reached.

An interesting feature appears when comparing Figs 4 and 6. For redshifts above roughly 10, the Universe is still mostly neutral ( $Q_i \ll 1$ ), and yet for  $z$  between 15 and 10 a significant fraction of the final total magnetic field strength is already generated. It means that the first sources are quite efficient at generating magnetic fields in the IGM. This is consistent with the fact that this mechanism operates in neutral regions: at these redshifts, the Strömgren spheres do not overlap yet, and the mechanism around each source works maximally. On the contrary, later on, less magnetic field is generated relatively to the number of sources which ionize the IGM.

Comparing the three curves in Fig. 6, we observe the following behaviour: the more strongly ionizing the sources are [corresponding to higher  $f_{\text{eff}}$ , i.e. either stars form very efficiently (high  $f_*$ ) or photons are not trapped (high  $f_{\text{esc}}$ )], the more magnetic fields are generated. Although it may seem obvious, it is not so simple because of the two following reasons. First, the stronger the sources, the more efficiently they reionize the Universe and the shorter the duration of the EoR is (and indeed, the plateau is reached earliest in the red case, and latest in the blue case). There is thus less time for the mechanism to operate. Secondly, as mentioned in the beginning of section 2, one should be cautious with the ‘naive’ and incorrect intuition that more powerful sources should generate stronger fields, since what matters in this mechanism is the compromise between having a high rate of photoionizations but also a high density of photons. In fact, the behaviour mentioned above can be accounted for as follows. In the case of the red curve, because the Universe is reionized early (cf. Fig. 4) the sources form in a medium with high density, and thus have small Strömgren spheres, so that in this case they generate strong magnetic fields. Since the neutral hydrogen density decreases as the Universe expands, the magnetic field generations are less efficient in the green and blue cases in which the source production is delayed with respect to the red case.

At the end of this section, it is worth mentioning how the total strength of the field (i.e. the level of the plateau in Fig. 6) depends on other parameters in our models. The most crucial ones are the boundaries of the integrals containing the mass parameters  $m$  and  $M$ , since they determine which clouds and which sources can contribute to the

magnetic field generation, through equations (10), (15) and (17). At the high end of the mass range, it turns out that the precise value of  $M_{\max}$  does not matter as long as it is large enough (in our model, we take it equal to  $10^{16}M_{\odot}$ ) since the mass function plummets at such large masses. Conversely, as previously mentioned, the lower boundary  $M_*$  for  $M$  is directly fixed by the physics of atomic cooling for star formation to be effective. For the mass  $m$  of the DM clouds containing neutral gas, the constraints on the upper bound discussed in section 2.2 are not very constraining. Indeed, if in fact one takes into account clouds with exaggerated (non-physical) sizes, the result is not very much changed because these overdensities are so large that they have very small density gradients, which is the key element of the present magnetogenesis mechanism, and thus do not generate important magnetic fields. For the lower limit of the parameter  $m$ , while we already provided physical arguments to constrain its value in section 2.2 to  $10^4 M_{\odot}$ , we also evaluated its impact on the total strength of the magnetic field by exploring a reasonably broader range of values. We found that the total magnetic field strength gradually increases as  $m_{\min}$  goes down. This is natural since in that case we are taking more and smaller neutral gas clouds into account. Decreasing  $m_{\min}$  down to the (redshift dependent) Jeans mass increases the resulting magnetic strength by less than 16 percent with respect to the fiducial value. On the contrary, including the effect of the streaming velocity between baryons and DM increases the filtering mass roughly by an order of magnitude. Since this suppresses neutral gas clouds in small DM haloes, it decreases the resulting magnetic strength, roughly by a factor of 2.

#### 4 DISCUSSION

Clearly, our model for the global magnetization of the Universe during the EoR is simplistic in several aspects and may be improved in different ways. However, given the high complexity of the underlying physics and context, the advantage of this analytic approach is that it helps disentangling the problem by explicating the main elements that determine the overall numerical value of the strength of the field, and provides us with an understanding of how they are at play, before resorting to numerical simulations. It is also an important first approach to the problem because it offers the valuable advantage of showing where the difficulties in the modelling are, in the perspective of a more refined approach.

Let us now briefly discuss points that we have not directly addressed in our model and try to assess whether they result in overestimating or underestimating the generated field. Note however that despite these, this work already gives a pertinent hint of the correct order of magnitude.

It has been shown in DL15 that the physical mechanism at the heart of our model is more efficient in underdense, rather than overdense regions of the IGM. Indeed, photons are less absorbed there, so they travel further and interact within more extended regions. Also, at a given distance from the source and with a given density gradient, the strength of the locally generated field is larger in the underdense case than in the overdense case since more photons reach that distance. In this paper, for simplicity, we considered only overdensities to model the clumpiness of the

IGM. We therefore neglected the a priori important contribution of the underdense regions between those clumps. A precise modelling of the profile of those regions is out of the scope of this work, but crudely speaking, since in our present model we did not consider roughly half of the neutral density gradients in the IGM, we estimate that the values of the generated field derived here could be actually doubled due to this.

In DL15, the authors justify that since the mechanism is assumed to operate around single sources during 100 Myr, it is relevant to consider, in a first approach, that the Strömgren spheres have reached their steady state. We followed this approach in this paper. However, whether this results in an overestimation or an underestimation of the overall mean generated magnetic field is not obvious. Indeed, in the transitory phase during which the Strömgren sphere grows, photons reaching the IGM are less geometrically diluted, so that the mechanism is very efficient closer to the source. At the same time, it is then less efficient further away, since photons above the hydrogen ionization threshold are in this case more absorbed than once the sphere has reached its steady state size. This work implicitly assumes that these two effects average out when we estimate the mean magnetic field, sticking to statistical information only.

In equation (17), we introduced a factor  $1 - Q_i$  to take into account the fact that the fraction of neutral gas decreases as sources switch on. However, we used equation (10) for the generated energy around each source, which is in principle only valid for an isolated source. To refine further the model, we would need to take into account the effect of neighbouring sources. This would not be as straightforward as it may seem, since we would need to model carefully how the field is generated in and around clouds that are illuminated by multiple sources, i.e. for instance how equation (3) for the generated field is modified when the radiation field is not unidirectional. This is best investigated probably through numerical simulations, which are actually under study for a forthcoming publication (Durrive & Aubert 2017, in preparation).

In this paper, we have not considered all the elements sourcing magnetic fields by photoionization. Indeed, as detailed in DL15, local inhomogeneities in the electron fraction as well as asphericity of the Strömgren regions also contribute to generating magnetic fields in the neutral IGM during EoR, in addition to the neutral hydrogen inhomogeneities that we have considered here. Asphericities of the Strömgren regions are probably a very important contribution since they induce potentially strong differences between adjacent lines of sight<sup>2</sup> directly near the ionization front, i.e. where the photon number density in the IGM is the largest. Once these transverse gradients exist, they are, in general, maintained all along the radial direction from the source. Therefore, we expect that contribution to yield non-negligible magnetic strengths not only locally, but also on extended distances. This is another reason to hypothesize that the value of the global magnetic field derived in this paper may be quite an underestimate.

<sup>2</sup> Such differences are key for the electric field to possess a curl, thus for the induction of magnetic fields, as detailed in DL15.

In comparison with other astrophysical processes operating during the EoR, let us first mention the work of Subramanian et al. (1994) and Gnedin et al. (2000). These authors explored the efficiency of the Biermann battery operating as ionization fronts travel through overdensities. The values we obtain for the generated magnetic field are just slightly lower than the values obtained in the Gnedin et al. (2000) study, and somewhat larger than those of Subramanian et al. (1994). However, in those studies, fields with significant strengths are generated essentially locally, in dense structures while, as already emphasized in DL15, the present mechanism, based on momentum transfer between photons and initially bound electrons, naturally generates the magnetic seeds deep in the neutral IGM, into which X and UV photons actually penetrate. Also, in Gnedin et al. (2000), the strengths reported in protogalactic structures are reached after amplification due to gas compression has taken place. The values we have obtained here are obtained directly, *without additional processing*. Though turbulence in the neutral IGM during the EoR is not well observationally constrained yet, simulations have shown that copious amounts of turbulent motions arise naturally during the formation of the first galaxies (Greif et al. 2008; Sur et al. 2012). Similarly, mechanical feedback associated with the formation and evolution of large-scale structure in the post-reionization universe does inject turbulence into the IGM (Rauch et al. 2001; Ryu et al. 2008; Oppenheimer & Davé 2009; Evoli & Ferrara 2011; Iapichino et al. 2011; Ravi et al. 2016). Stretching, twisting and folding of magnetic field lines associated with the compressive and shearing motions of turbulence will in reality amplify and reorganize the seed fields obtained in this study, and bring them to the strengths detected in the present-day, structured IGM (e.g. Ryu et al. 2008; Schleicher et al. 2010; Sur et al. 2012; Vazza et al. 2014, and references therein). Within cosmic voids, collision-less plasma instabilities have the potential to amplify rapidly the magnetic seed fields (e.g. Falceta-Gonçalves & Kowal 2015), and bring them to and maintain them above the lower limits suggested by the observation of distant blazars and cited in the Introduction section (see also Finke et al. 2015).

Another interesting process that may begin already during the EoR is the spontaneous emission of aperiodic turbulent magnetic field fluctuations in the initially unmagnetized intergalactic plasma (Schlickeiser & Yoon 2012; Schlickeiser 2012; Schlickeiser & Felten 2013). Taking into account viscous damping from collisional processes, those fluctuations may reach strengths of the order of  $10^{-12}$  G in protogalactic clouds, where they can contribute to seeding the amplifying dynamo actions relevant to galactic magnetic fields. In the post-reionization plasma of cosmic voids they may reach  $10^{-21}$  G (Schlickeiser & Yoon 2012). Those strengths can be larger, up to the  $10^{-16}$  G level in fully ionized regions (in partially ionized regions, a somewhat stronger damping reduces that level), when collective effects enter the game (Schlickeiser & Felten 2013). However, while this mechanism may operate throughout the entire IGM, the resulting magnetic field fluctuations are generated on very small scales, smaller than  $10^{-4}$  pc, on time-scales of the order of  $10^{10}$  years. On the contrary, the mechanism of global IGM magnetization examined in this paper relies on the detailed process of photon-to-electron momentum transfer that creates magnetic field seeds on scales comparable to the distance

between ionizing sources, as detailed in section 3, and with a coherence essentially set by the size of the gas inhomogeneities present in the IGM (see also Durriue & Langer 2015). In addition, it magnetizes the entire IGM, including those regions that will become cosmic voids, by the end of the EoR, that is within the first billion years of the Universe.

In conclusion, our model suggests that the Universe may be globally magnetized to the order of *at least* a few  $10^{-20}$  G (comoving) by this mechanism<sup>3</sup>. Note that this order of magnitude falls within the range of values obtained in the numerical applications performed in DL15 for clouds close to a single source. This work thus shows that the strength of the fields generated by this mechanism is not only important locally, i.e. around isolated sources, but also in a global context, i.e. that the typical distribution of sources, the clumpiness of the IGM and the typical duration of EoR, allow for this mechanism to be of cosmological relevance. As a final note, it is an exciting perspective that such magnetic seeds might be directly measurable with the Square Kilometre Array by means of the method based on 21-cm tomography proposed in Venumadhav et al. (2017) and Gluscevic et al. (2017).

## ACKNOWLEDGMENTS

The authors are grateful to the organizers of the conference and workshops ‘Origin, Evolution, and Signatures of Cosmological Magnetic Fields’ held in June-July 2015 at NORDITA where this work was initiated. JBD acknowledges financial support by the P2IO LabEx (ANR-10-LABX-0038) in the framework ‘Investissements d’Avenir’ (ANR-11-IDEX-0003-01) managed by the French National Research Agency (ANR). This work was supported in part by JSPS Grants-in-Aid for Scientific Research under Grant Nos. 25287057 (N.S.), 15H05890 (N.S.) and 15K17646 (H.T.).

## REFERENCES

- Aleksić J., et al., 2010, *Astronomy & Astrophysics*, 524, A77  
 Arlen T. C., Vassilev V. V., Weisgarber T., Wakely S. P., Shafi S. Y., 2014, *The Astrophysical Journal*, 796, 18  
 Arshakian T. G., Beck R., Krause M., Sokoloff D., 2009, *Astronomy & Astrophysics*, 494, 21  
 Beck R., 2011, in Aharonian F. A., Hofmann W., Rieger F. M., eds, 25th Texas Symposium on Relativistic Astrophysics (Texas 2010). AIP Conference Proceedings. pp 117–136 ([arXiv:1104.3749](https://arxiv.org/abs/1104.3749)), doi:10.1063/1.3635828  
 Beck R., 2016, *The Astronomy and Astrophysics Review*, 24, 4  
 Beck A. M., Hanasz M., Lesch H., Remus R.-S., Stasyszyn F. A., 2013, *Monthly Notices of the Royal Astronomical Society*, 429, L60  
 Biermann L., 1950, *Zeitschrift für Naturforschung A*, 5, 65  
 Birk G. T., Wiechen H., Lesch H., 2002, *Astronomy and Astrophysics*, 393, 685  
 Blasi P., Burles S., Olinto A. V., 1999, *The Astrophysical Journal*, 514, L79  
 Brandenburg A., Subramanian K., 2005, *Physics Reports*, 417, 1  
 Bret A., 2009, *The Astrophysical Journal*, 699, 990

<sup>3</sup> Potentially larger values could be reached due to possible kinetic effects (Munirov & Fisch 2017).

- Broderick A. E., Chang P., Pfrommer C., 2012, *The Astrophysical Journal*, 752, 22
- Brown S., et al., 2017, *Monthly Notices of the Royal Astronomical Society*, 468, 4246
- Chang P., Broderick A. E., Pfrommer C., Puchwein E., Lamberts A., Shalaby M., Vasil G., 2016, *The Astrophysical Journal*, 833, 118
- Chluba J., Paoletti D., Finelli F., Rubiño-Martín J. A., 2015, *Monthly Notices of the Royal Astronomical Society*, 451, 2244
- Daly R. A., Loeb A., 1990, *The Astrophysical Journal*, 364, 451
- Dermer C. D., Cavadini M., Razzaque S., Finke J. D., Chiang J., Lott B., 2011, *The Astrophysical Journal*, 733, L21
- Dolag K., Kachelriess M., Ostapchenko S., Tomàs R., 2011, *The Astrophysical Journal*, 727, L4
- Durrer R., Neronov A., 2013, *The Astronomy and Astrophysics Review*, 21
- Durrive J.-B., Aubert D., 2017, in preparation
- Durrive J.-B., Langer M., 2015, *Monthly Notices of the Royal Astronomical Society*, 453, 345
- Evoli C., Ferrara A., 2011, *Monthly Notices of the Royal Astronomical Society*, 413, 2721
- Falceta-Gonçalves D., Kowal G., 2015, *The Astrophysical Journal*, 808, 65
- Fenu E., Pitrou C., Maartens R., 2011, *Monthly Notices of the Royal Astronomical Society*, 414, 2354
- Feretti L., Giovannini G., Govoni F., Murgia M., 2012, *The Astronomy and Astrophysics Review*, 20, 54
- Ferrario L., Melatos A., Zrake J., 2015, *Space Science Reviews*, 191, 77
- Finke J. D., Reyes L. C., Georganopoulos M., Reynolds K., Ajello M., Fegan S. J., McCann K., 2015, *The Astrophysical Journal*, 814, 20
- Furlanetto S. R., Loeb A., 2001, *The Astrophysical Journal*, 556, 619
- Glover S., 2013, in Wiklind T., Mobasher B., Bromm V., eds, *Astrophysics and Space Science Library*, Vol. 396, *The First Galaxies – Theoretical Predictions and Observational Clues*. Springer Berlin Heidelberg, pp 103–174
- Gluscevic V., Venumadhav T., Fang X., Hirata C., Oklopčić A., Mishra A., 2017, *Physical Review D*, 95, 083011
- Gnedin N. Y., Hui L., 1998, *Monthly Notices of the Royal Astronomical Society*, 296, 44
- Gnedin N. Y., Ferrara A., Zweibel E. G., 2000, *The Astrophysical Journal*, 539, 505
- Greif T. H., Johnson J. L., Klessen R. S., Bromm V., 2008, *Monthly Notices of the Royal Astronomical Society*, 387, 1021
- Gruzinov A., 2001, *The Astrophysical Journal*, 563, L15
- Harrison E. R., 1970, *Monthly Notices of the Royal Astronomical Society*, 147, 279
- Harrison E. R., 1973, *Physical Review Letters*, 30, 188
- Hayes M., Schaerer D., Östlin G., Mas-Hesse J. M., Atek H., Kunth D., 2011, *The Astrophysical Journal*, 730, 8
- Iapichino L., Schmidt W., Niemeyer J. C., Merklein J., 2011, *Monthly Notices of the Royal Astronomical Society*, 414, 2297
- Iwata I., et al., 2009, *The Astrophysical Journal*, 692, 1287
- Kempf A., Kilian P., Spanier F., 2016, *Astronomy & Astrophysics*, 585, A132
- Kim E.-J., Olinto A. V., Rosner R., 1996, *The Astrophysical Journal*, 468, 28
- Kronberg P. P., Lesch H., Hopp U., 1999, *The Astrophysical Journal*, 511, 56
- Kulsrud R. M., Zweibel E. G., 2008, *Reports on Progress in Physics*, 71, 046901
- Langer M., Puget J.-L., Aghanim N., 2003, *Physical Review D*, 67, 1
- Langer M., Aghanim N., Puget J.-L., 2005, *Astronomy & Astrophysics*, 443, 367
- Lazar M., Schlickeiser R., Wielebinski R., Poedts S., 2009, *The Astrophysical Journal*, 693, 1133
- Loeb A., Furlanetto S. R., 2013, *The First Galaxies in the Universe*. Princeton Series in Astrophysics, Princeton University Press
- McQuinn M., 2016, *Annual Review of Astronomy and Astrophysics*, 54, 313
- Medvedev M. V., Silva L. O., Kamionkowski M., 2006, *The Astrophysical Journal*, 642, L1
- Mellema G., Iliev I. T., Pen U. L., Shapiro P. R., 2006, *Monthly Notices of the Royal Astronomical Society*, 372, 679
- Menzler U., Schlickeiser R., 2015, *Monthly Notices of the Royal Astronomical Society*, 448, 3405
- Mishustin I. N., Ruzmaikin A. A., 1972, *Soviet Physics JETP*, 34, 233
- Mo H., van den Bosch F. C., White S. D. M., 2010, *Galaxy Formation and Evolution*. Cambridge University Press
- Munirov V. R., Fisch N. J., 2017, *Physical Review E*, 95, 013205
- Naoz S., Barkana R., 2007, *Monthly Notices of the Royal Astronomical Society*, 377, 667
- Naoz S., Narayan R., 2013, *Physical Review Letters*, 111, 051303
- Neronov A., Vovk I., 2010, *Science*, 328, 73
- Oppenheimer B. D., Davé R., 2009, *Monthly Notices of the Royal Astronomical Society*, 395, 1875
- Pandey K. L., Sethi S. K., 2013, *The Astrophysical Journal*, 762, 15
- Peebles P. J. E., 1980, *The large-scale structure of the universe*. Princeton University Press
- Planck Collaboration 2016a, *Astronomy & Astrophysics*, 594, A1
- Planck Collaboration 2016b, *Astronomy & Astrophysics*, 594, A13
- Planck Collaboration 2016c, *Astronomy & Astrophysics*, 594, A19
- Planck Collaboration 2016d, *Astronomy & Astrophysics*, 596, A108
- Press W. H., Schechter P., 1974, *The Astrophysical Journal*, 187, 425
- Pshirkov M. S., Tinyakov P. G., Urban F. R., 2016, *Physical Review Letters*, 116, 191302
- Pudritz R. E., Silk J., 1989, *The Astrophysical Journal*, 342, 650
- Raiter A., Schaerer D., Fosbury R., 2010, *Astronomy & Astrophysics*, 523, A64
- Rauch M., Sargent W. L. W., Barlow T. A., 2001, *The Astrophysical Journal*, 554, 823
- Ravi V., et al., 2016, *Science*, 354, 1249
- Rees M. J., 1987, *Royal Astronomical Society, Quarterly Journal*, 28, 197
- Ryu D., Kang H., Biermann P. L., 1998, *Astronomy & Astrophysics*, 335, 19
- Ryu D., Kang H., Cho J., Das S., 2008, *Science*, 320, 909
- Ryu D., Schleicher D. R. G., Treumann R. A., Tsagas C. G., Widrow L. M., 2012, *Space Science Reviews*, 166, 1
- Saga S., Ichiki K., Takahashi K., Sugiyama N., 2015, *Physical Review D*, 91, 123510
- Schaerer D., 2002, *Astronomy & Astrophysics*, 382, 28
- Schleicher D. R. G., Banerjee R., Sur S., Arshakian T. G., Klessen R. S., Beck R., Spaans M., 2010, *Astronomy & Astrophysics*, 522, A115
- Schlickeiser R., 2012, *Physical Review Letters*, 109, 261101
- Schlickeiser R., Felten T., 2013, *The Astrophysical Journal*, 778, 39
- Schlickeiser R., Shukla P. K., 2003, *The Astrophysical Journal*, 599, L57
- Schlickeiser R., Yoon P. H., 2012, *Physics of Plasmas*, 19, 022105
- Schober J., Schleicher D. R. G., Klessen R. S., 2013, *Astronomy & Astrophysics*, 560, A87
- Sironi L., Giannios D., 2014, *The Astrophysical Journal*, 787, 49
- Subramanian K., 2016, *Reports on Progress in Physics*, 79, 076901
- Subramanian K., Narasimha D., Chitre S. M., 1994, *Monthly Notices of the Royal Astronomical Society*, 271, L15

- Sur S., Federrath C., Schleicher D. R. G., Banerjee R., Klessen R. S., 2012, *Monthly Notices of the Royal Astronomical Society*, 423, 3148
- Tashiro H., Sugiyama N., 2006, *Monthly Notices of the Royal Astronomical Society*, 368, 965
- Tavecchio F., Ghisellini G., Bonnoli G., Foschini L., 2011, *Monthly Notices of the Royal Astronomical Society*, 414, 3566
- Tseliakhovich D., Barkana R., Hirata C. M., 2011, *Monthly Notices of the Royal Astronomical Society*, 418, 906
- Vallée J. P., 2011, *New Astronomy Reviews*, 55, 91
- Varalakshmi C., Nigam R., 2017, *Astrophysics and Space Science*, 362, 16
- Vazza F., Brüggem M., Gheller C., Wang P., 2014, *Monthly Notices of the Royal Astronomical Society*, 445, 3706
- Venters T. M., Pavlidou V., 2013, *Monthly Notices of the Royal Astronomical Society*, 432, 3485
- Venumadhav T., Oklopčić A., Gluscevic V., Mishra A., Hirata C. M., 2017, *Physical Review D*, 95, 083010
- Wasserman I., 1978, *The Astrophysical Journal*, 224, 337
- Widrow L. M., 2002, *Reviews of Modern Physics*, 74, 775
- Widrow L. M., Ryu D., Schleicher D. R. G., Subramanian K., Tsagas C. G., Treumann R. a., 2012, *Space Science Reviews*, 166, 37
- Wise J. H., Cen R., 2009, *The Astrophysical Journal*, 693, 984
- Wise J. H., Demchenko V. G., Halicsek M. T., Norman M. L., Turk M. J., Abel T., Smith B. D., 2014, *Monthly Notices of the Royal Astronomical Society*, 442, 2560
- Zackrisson E., Rydberg C.-E., Schaerer D., Östlin G., Tuli M., 2011, *The Astrophysical Journal*, 740, 13
- Zucca A., Li Y., Pogosian L., 2017, *Physical Review D*, 95, 063506

## APPENDIX A: EVOLUTION OF MAGNETIC FIELDS

We provide here the derivation of equation (17), the average magnetic energy density (physical) generated during the EoR.

Assuming magnetic flux freezing, we must account for the fact that any magnetic field newly generated in the IGM is subsequently adiabatically diluted by cosmic expansion. Consequently, not taking into account any possible dissipation or amplification at this point, at a given redshift  $z$ , during a redshift interval  $dz$  the physical (hence subscripts ‘p’) magnetic energy density varies as

$$d\left(\frac{B_p^2}{8\pi}\right) = \frac{4}{1+z} \frac{B_p^2}{8\pi} dz + de, \quad (\text{A1})$$

where the first term on the right-hand side corresponds to adiabatic dilution, and  $de$  is a source term, corresponding to the energy density generated during  $dz$ . We have

$$de = \frac{de}{dt} \frac{dt}{dz} dz \quad (\text{A2})$$

where the time-redshift correspondence is given by the expansion rate at redshift  $z$ , according to

$$\frac{dt}{dz} = -\frac{1}{(1+z)H(z)}. \quad (\text{A3})$$

We model the energy generated during  $dt$  as

$$\frac{de}{dt} = (1 - Q_i) \int_{M_*}^{M_{\max}} dM E_M g_{\text{gl}} \frac{dn_M}{dM}. \quad (\text{A4})$$

Indeed, we construct this term in analogy with the expression for the volume filling factor (15) but with  $E_M$  in place

of  $V_{\text{ion}}$ : we weigh the number density of haloes by  $g_{\text{gl}}$  so that once a source switches on, we add its contribution, but at each time step, we add the contribution only of the newly born sources as required. However, equation (10) for  $E_M$  that we derived in the previous section corresponds to the energy generated in the IGM by an *isolated* source, while in practice when considering a distribution of sources, we must take into account the fact that Strömgren spheres overlap. This is essential since our mechanism is efficient only in neutral regions, so that we expect its efficiency to decrease as Reionization progresses. Hence, we cannot simply add up the contribution of sources contained in DM haloes with equation (10) without care, otherwise we would overestimate the field generation. We thus introduce in equation (A4) the factor  $1 - Q_i$ , which reduces the fraction of neutral Hydrogen in the model as time passes, consistently with the amount of sources switching on since  $Q_i$  is given by equation (15).

Now, the relation given by equation (A1) yields the differential equation governing the evolution of the physical magnetic energy density. It is convenient to put together the term on the left-hand side with the first term on the right-hand side, and rewrite equation (A1) as

$$(1+z)^4 \frac{d}{dz} \left[ (1+z)^{-4} \frac{B_p^2}{8\pi} \right] = \frac{de}{dz} \quad (\text{A5})$$

so that it can be easily integrated. With equations (A2), (A3) and (A4), we finally get that the mean magnetic energy density (physical) generated by photoionizations during EoR evolves with redshift according to equation (17).

This paper has been typeset from a  $\text{\TeX}/\text{\LaTeX}$  file prepared by the author.